ME445 project 2023 GROUP 02

✉ **Email addresses:**
[1]paolo.giaretta@epfl.ch

GIARETTA, Paolo[1]
DE BAZELAIRE, Simon[2]
CLERGEOT, Marion[3]

Abstract

In "Airfoil Aerodynamics in Ground Effect for Wide Range of Angles of Attack", Qu, Qiulin, et al. (AIAA Journal, 2015), the effect of the ground is studied for a NACA 4412 airfoil for various angles of attack and ride heights using Reynolds-Averaged Navier Stokes (RANS) simulations. The main aim is to assess the effect of the ground on the lift properties of the airfoil. Our motivation for choosing this particular paper reflects our interest in expanding the aerodynamics theories seen in lectures to the peculiar and challenging ground effect regime. In this report, Potential flow and Thin Airfoil theories are used to compute lift and pressure coefficient distributions respectively. The obtained solutions are then compared to the viscous simulations. Our results show that trends in the unbounded and ground effect cases can be replicated with inviscid theories, although large differences may emerge as a result of angle of attack and other underlying assumptions.

Introduction

Great focus is placed in the selected paper on the ground effect for different angles of attack and ride heights. The physical model relies on the assumption that the ground effect is fundamental only when the ride height is such that $h/c < 1$, where h is the distance of the trailing edge to the ground and c is the airfoil chord. Numerical results are compared to experimental data of a widely-used racing car airfoil.

This paper aims to study 2 different effects :
The first is to use the thin airfoil theory to study the unbounded flow. We will relax the standard assumption of placing the vortex distribution on the chordline and see if this improvement performs better than the classical version of this theory for different angles of attack. We will study the difference in pressure coefficient between the lower and upper surfaces ($\Delta Cp = Cp_{\text{lower surface}} - Cp_{\text{upper surface}}$) for different values of angle of attack (α = 4, 8, 16 and 18 °). The results will be compared with the CFD simulations from the selected paper (Fig.1.a).

The second effect we want to study is the ground effect. For this, we will use the potential flow theory to calculate the lift coefficient (C_l) curve as a function of the angle of attack (α). The height is adimensionalized as a function of chord length (c). The ride heights considered in this study are $\frac{h}{c}$ = 0.4, 0.8, 1.0 and ∞ (i.e. without ground effect). The aim is

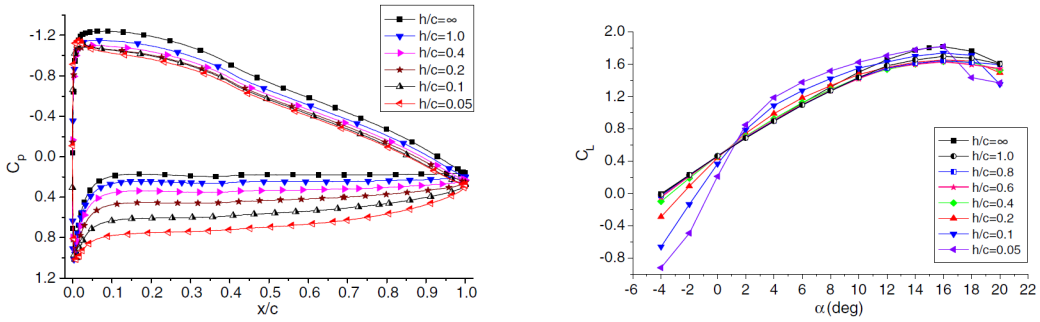

Figure 1. Pressure coefficient distribution (Fig.9.a of the selected paper) to be reproduced with Thin Airfoil theory. Lift coefficient curves for different ride heights (Fig.5.a of the selected paper) to be reproduced with Potential flow theory.

---

to reproduce the observed trend in the lift coefficient curves for the viscous simulations (Fig.1.b).

In the following sections, we start by stating some necessary preliminary assumptions when applying these inviscid flow theories. Successively, we present the details for airfoil parametrization and delve into the details of the algorithms and MATLAB routines employed. At the end, the results are presented and compared with the CFD simulations in the paper, highlighting the limitations of these two theories and their sensitivity to underlying assumptions.

Description of the problem and numerical techniques

Preliminary assumptions

The following necessary assumptions are taken when applying thin airfoil theory and potential flow theory:

- **Steadiness of the flow**. This assumption is reflected by the simulation conditions in the paper (Qiulin Qu, Liu, and Agarwa (April 2015)). Even if at a Reynolds number of $6 \cdot 10^6$ the flow presents turbulent behaviour, hence it is intrinsically unsteady, we assume the average flow can be approximated as completely steady.
- **Inviscidity**. At these Reynolds values viscous effects present a significant role in the boundary layer. The outer flow can therefore be approximated as potential. Given that we are interested in pressure-based forces we completely neglect the fluid viscosity in this analysis.
- **Imcompressibility**. A fluid may be considered incompressible for $Ma < 0.3$. The asymptotic velocity is $Ma_\infty = 0.26$. When the fluid passes over the airfoil, the velocity can reach peaks up to $Ma = 0.38$. This leads to a maximum difference in density of 7%. Even though we neglect compressibility, for large angles of attack the effects of compressibility may not be entirely negligible and may introduce additional sources of error.

Data extraction and airfoil parametrization

To compare the aerodynamic theories it is necessary to extract the datapoints from the paper and transform them into a MATLAB-compatible form. The online data sampling tool www.graphreader.com v2 has been used. The tool allows uploading a plot image and extracting individual data points. The tool allows for post-processing such as data smoothening and interpolation to better match the sampled curve with the original one. The data points are then saved in MATLAB in the form of a `.mat` file. In the scope of this analysis, the $C_l - \alpha$ and $C_p - x$ curves are extracted for a range of ground distances h/c $(0.4,\ 0.8,\ 1.0,\ \infty)$ and angles of attack ($\alpha = 4°,\ 8°,\ 16°,\ 18°$).

The NACA 4412 airfoil is parametrized by the method outlined in "Theory of wing sections: including a summary of airfoil data" (pag.111-114) (Abbott and Von Doenhoff, 2012). The four-digit NACA airfoil presents a maximum camber of 4% $(m = 0.04)$ at 40% of the chord $(p = 0.4)$ with a maximum thickness of 12% $(t = 0.12)$. For a NACA airfoil, the meanline elevation y_{ml} can be computed from the chordwise coordinate x as in Eq.1. The chordwise thickness distribution y_t can be computed analytically from the NACA 4-digit expansion as in Eq.2. The upper and lower airfoil surfaces are reconstructed by applying the thickness distribution in the pointwise normal direction to the meanline.

$$y_{ml} = \begin{cases} \frac{m}{p^2}\left(2px - x^2\right), & x \leq p \\ \frac{m}{1-p^2}\left((1-2p) + 2px - x^2\right), & x > p \end{cases} \tag{1}$$

$$y_t = 5\,t\,\left(0.2969\sqrt{x}\ -\ 0.126x - 0.3516x^2 + 0.2843x^3 - 0.1036x^4\right) \tag{2}$$

Thin Airfoil Theory

We decided to apply first the thin airfoil theory to investigate the unbounded flow and limits of applicability of this theory. For this analysis, the flow is assumed to be potential and the airfoil is approximated by its meanline. The velocity field and airfoil pressure distribution result from the vortex distribution k placed on the meanline. First, we present the classical trigonometric approximate solution for the unbounded flow over the airfoil. Secondly, we will present a method based on the work presented in "Discrete Vortex Method-Based Model for Ground-Effect Studies" (Mondal and Balakrishnan, 2014). This approach challenges some assumptions of the classical thin airfoil theory and allows us to relax the assumption of small camber and angle of attack.

Classical Thin Airfoil Theory

Two main assumptions are necessary in the standard formulation of the thin airfoil theory. The airfoil angle of attack and thickness are considered to be small ($\alpha \ll 1,\ t \ll c$). Viscous effects may be neglected in this approximation and a potential flow solution (generated by a continuous meanline vortex distribution) is considered. The small thickness and camber of the airfoil justify the approximation of projecting the vortex distribution onto the chordline and looking for solutions for the chord-wise vorticity distribution. The

vorticity distribution can be computed by imposing the boundary conditions of no penetration at the airfoil meanline (approximated by the chord) and the Kutta Condition.
In the trigonometric approach, the solution can be expanded as an infinite series of trigonometric contributions. First, the meanline profile derivative is expanded as a cosine trigonometric polynomial (Eq.3, Eq. 4).

$$\frac{dy_{ml}}{dx} = A_0 + \sum_{n=1}^{\infty} A_n cos(n\theta) \quad , \quad x = \frac{1 - cos(\theta)}{2} \tag{3}$$

$$A_0 = \frac{1}{\pi} \int_0^{\pi} \frac{dy_{ml}}{dx} dx \qquad A_n = \frac{2}{\pi} \int_0^{\pi} \frac{dy_{ml}}{dx} cos(n\theta)\, dx \tag{4}$$

The circulation distribution is then a function of angle of attack (α), asymptotic flow velocity (U_∞) and the obtained Fourier coefficients (Eq.5).

$$k = 2U_\infty \left[\left(\alpha - A_0\right) \frac{cos(\theta) + 1}{sin(\theta)} + \sum_{n=1}^{\infty} A_n sin(n\theta) \right] \quad , \quad x = \frac{1 - cos(\theta)}{2} \tag{5}$$

Once these quantities are calculated the curves for the difference in pressure coefficient between the upper and lower surfaces (ΔC_p) are calculated as follows:

$$\Delta C_p = \frac{\Delta P}{1/2 \rho \mathrm{U}_\infty^2} = 2 \frac{k}{U_\infty} \tag{6}$$

This method has been implemented by discretizing the airfoil into a finite set of points and calculating the trigonometric coefficients by numerical integration of Eq.4 with the trapezoidal method with the MATLAB built-in function `trapz`. The circulation distribution is calculated by truncating the infinite summation to the first N terms.

Discrete Vortex Method

Following (Mondal and Balakrishnan, 2014), we used the Discrete Vortex Method to solve for the flow over the airfoil. One first difference with the classical thin airfoil approach is the placement of the vortex distribution exactly on the camberline and not projected onto the chord (Fig.2). The method is well-suited even for airfoils with relatively large maximal cambers (assuming that the flow field can still be treated as potential). The meanline is discretized into N consecutive segments. Each segment presents a **vortex** point at $1/4$ of the segment length and a **collocation** point at $3/4$ of the segment length. At each vortex point, a vortex source with circulation $\Gamma_k,\ k = 1, \ldots, N$ is introduced. At each collocation point the normal component to the segment is calculated as a function of the discrete circulation distribution and asymptotic flow U_∞. A NxN system of equations for the circulations is obtained by imposing the non-penetration boundary condition at all collocation points. The linear system of equations is the following:

$$\left[\sum_{j=1}^{N} (u,\, v)_{ij} + \left(U_\infty,\, 0\right) \right] \cdot \hat{n}_i = 0 \quad , \quad i = 1, \ldots, N \tag{7}$$

Where $(u,\ v)_{ij}$ is the velocity vector induced by the i-th vortex onto the j-th panel, $\left(U_\infty,\ 0\right)$ the asymptotic velocity and $\hat{n}_i$ the normal unit vector to the i-th panel. The complex velocity vector induced by each vortex is computed as:

$$(u - iv)_{ij} = \frac{\Gamma_j}{2\pi} \frac{\left(y_i - y_j\right) + i\left(x_i - x_j\right)}{\left(y_i - y_j\right)^2 + \left(x_i - x_j\right)^2} \tag{8}$$

To implement this method we first compute the linear system coefficients in the respective matrix form and solve for the discrete circulation distribution. From the circulation distribution, it is possible to reconstruct the total circulation, hence the lift coefficient by the Kutta-Joukowsky theorem (Eq. 9). Furthermore, it is possible to compute the whole velocity field by summing all vortex contributions at any query point in the flow field (Eq. 8). To determine the differential pressure coefficient distribution ΔC_p, we assume that each circulation Γ_i is uniformly distributed inside each meanline segment.

$$\begin{aligned} L &= -\rho U_\infty \Gamma = -\rho U_\infty \sum_{i=1}^{N} \Gamma_i \\ \Delta C_p &= -\frac{2k(s)}{U_\infty} \quad , \quad k(s)_i = \Gamma_i / \Delta s_i \end{aligned} \tag{9}$$

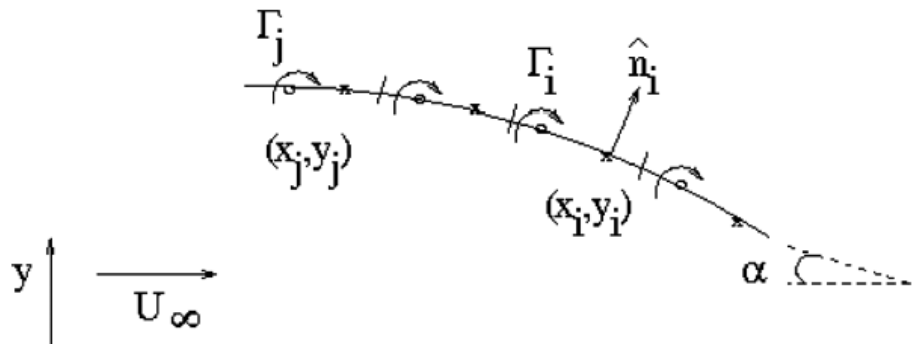

Figure 2. Discretization method employed in the Discrete Vortex Method (Mondal and Balakrishnan (2014)).

Potential Flow theory

We decided to use potential flow theory to investigate the effect of the ground on the airfoil $C_l - \alpha$ curve for a wide range of ground distances h/c (the adimensional distance of the trailing edge from the ground). The method of images is used to represent the effect of the ground in the potential flow analysis. This technique simulates the ground by introducing a new airfoil which is the mirror image of the first one to the ground. The flow field solution over the two airfoils presents a streamline over the ground surface due to the symmetry of the problem. Thus, the top half-plane solution can be interpreted as the complete flow field over an airfoil in ground effect.
The potential flow theory allows us to divide the full problem into two parts. First, we are

interested in finding a complex conformal map between two cylinders with circulation in the ζ-plane and the two mirror airfoils in the complex z-plane. Second, we compute the flow solution over the two cylinders. This solution can then be mapped back into the airfoil plane by the conformal map previously found. We will explain these two steps in the following sections.

Finding the conformal map

In this section, we will follow the work by DeLillo et al. in (DeLillo and Sahraei (2019), DeLillo, Horn, and Pfaltzgraff (1999), and DeLillo and Pfaltzgraff (1998)). The conformal mapping between the two airfoils and two cylinders is found in two steps. First, the airfoils are mapped to near-circular regions by two successive Karman-Trefftz maps that eliminate the sharp trailing edge angle of the NACA 4412 airfoils. Successively, an iterative Newton-like procedure finds an approximate conformal mapping between two cylinders of radii r_1, r_2 and centres c_1, c_2 and the two near-circular boundaries.

The Karman-Trefftz transformation is an everywhere conformal map except at a single point. If the point is carefully chosen as the trailing edge of one of the airfoils, it is possible to remove completely the sharp trailing-edge angle and map the airfoil to an almost circular shape. The equation of the Karman-Trefftz map is given in Eq.10 where beta is the internal trailing edge angle to be removed, z_1 the trailing edge coordinate mapped to ζ_1 and z_2 any point inside the airfoil close to the leading edge mapped to ζ_2.

$$\frac{\zeta - \zeta_1}{\zeta - \zeta_2} = \left(\frac{z - z_1}{z - z_2} \right)^{\frac{\pi}{2\pi - \beta}} \tag{10}$$

The conformal map to transform the two cylinders in the near-circular shapes obtained previously can be described approximately by Eq.11. The Fornberg-like algorithm developed by DeLillo et al. allows to obtain iteratively the unknown coefficients $a_{1,i}$, $a_{2,i}$ and cylinders parameters r_1, r_2, c_1, c_2. Please refer to (DeLillo, Horn, and Pfaltzgraff, 1999) for a step-by-step description of the iterative procedure. The necessary steps to map the original airfoils into two perfect cylinders are summarized in Fig.3.

$$f(\zeta) = \zeta + \sum_{i=1}^{N} a_{1,i} \left(\frac{r_1}{\zeta - c_1} \right)^i + a_{2,i} \left(\frac{r_2}{\zeta - c_2} \right)^i \tag{11}$$

Flow over two cylinders with circulation

The flow over the two cylinders can be obtained by repeated application of **Milne-Thomson circle theorem**, as outlined in Sahraei (2018) for the general n-cylinder problem. The full solution is obtained by starting with the full complex potential solution for the flow over a first cylinder with circulation Γ_1. It is then possible to introduce a second cylinder with circulation in the flow by applying the Milne-Thomson circle theorem. When the second cylinder is introduced, the streamlines of the first one are perturbed and no longer enclose a perfect circle. The circle theorem is then repeated to the first cylinder

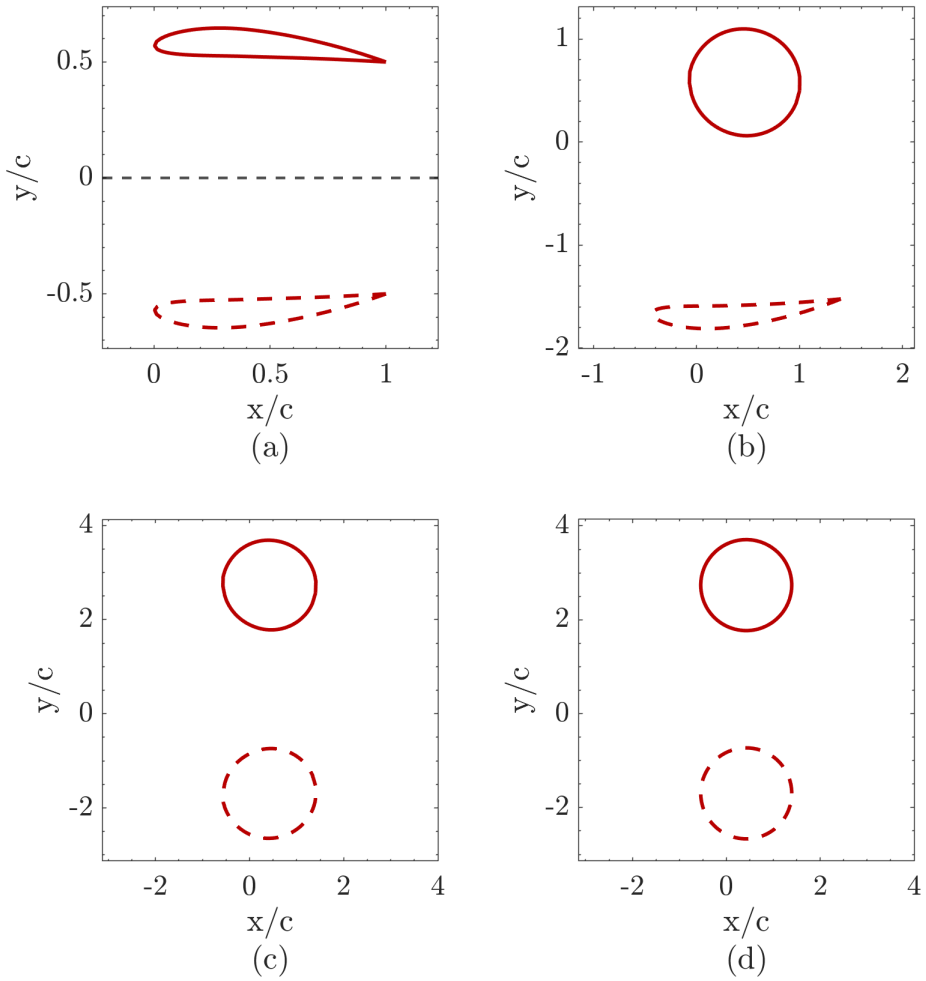

Figure 3. Necessary steps to map conformally two airfoils to two perfect cylinders for $\alpha = 4°$, $h/c = 0.5$. The airfoil in ground effect and its mirror image (a). Boundaries after the first Karman-Trefftz map (b). Boundaries after the second Karman-Trefftz map (c). Perfect cylinders after the Fornberg-like algorithm.

to re-establish the desired circular streamline. This procedure is applied alternating between the two cylinders until the desired convergence of the flow field is achieved. The Kutta conditions for each cylinder are imposed, obtaining a 2x2 system in the unknown circulations Γ_1, Γ_2. An example of a flow field obtained with this procedure is depicted in Fig.4.

The complex velocity and potential fields can be mapped back into the airfoils domain by first applying the conformal mapping to the quasi-circular domain and inverting both Karman-Trefftz transforms. Successively, the coefficient of lift can be calculated from the circulation around the airfoils by the Kutta-Joukowsky theorem. This procedure is repeated for the desired range of angles of attack and ground distances to assess the airfoil performance in this regime.

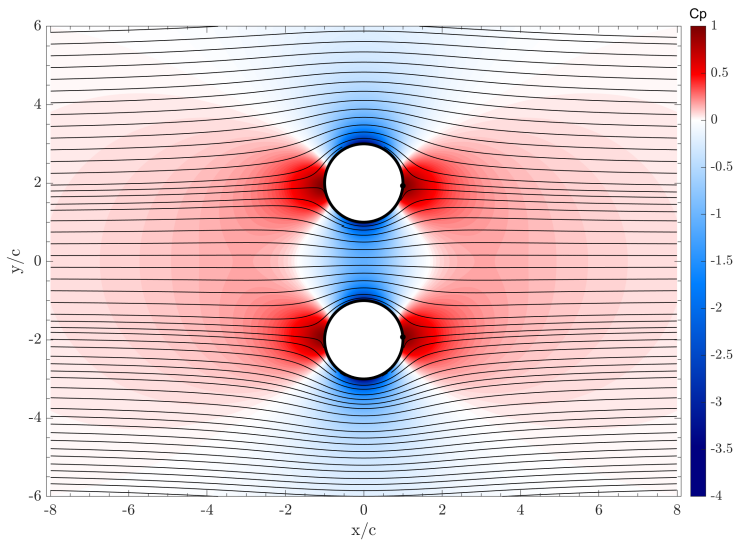

Figure 4. Flow over two cylinders with circulation. $r_1 = r_2 = 1$, $c_1 = 2i$, $c_2 = -2i$ The stagnation points where the Kutta Condition is imposed (black dots) are $\pm 4°$ from the horizontal.

Results & Discussion

Thin Airfoil Theory

The results of the classical thin airfoil theory and the Discrete Vortex Method for the unbounded flow over the NACA 4412 profile are depicted in Fig.5 for all angles of attack provided in the paper ($\alpha = 4°, 8°, 16°, 18°$).

For all angles of attack, the Discrete Vortex Method estimates a higher pressure distribution than the trigonometric approach. The discrepancy between the two theories becomes greater as the angle of attack is increased. This is to be expected as the projection of the vortex distribution onto the chord becomes less accurate at large angles of attack. There are notable differences between the thin airfoil approach and the CFD results from the paper. Most notably, both airfoil theories place an asymptotically infinite circulation distribution at the leading edge. This non-physical result is due to the almost infinite curvature of the streamlines at the leading edge when the airfoil is simply approximated by its meanline. The CFD results show a pronounced but finite spike in pressure at the rounded leading edge. For $4°$ and $8°$ angles of attack, the computed curves show a relatively similar trend to the paper ones. Neglecting the airfoil thickness leads to an underestimate of the pressure coefficient difference in the first half of the chord and an overestimation in the second half. At the trailing edge, all curves meet exactly with no pressure difference due to the imposed Kutta condition. For $16°$ and $18°$ angles of attack, the discrepancy between both thin airfoil theories and the CFD results becomes evident and the pressure differential is completely overestimated. At these large angles of attack viscous effects may not be therefore neglected in the study of pressure-based forces.

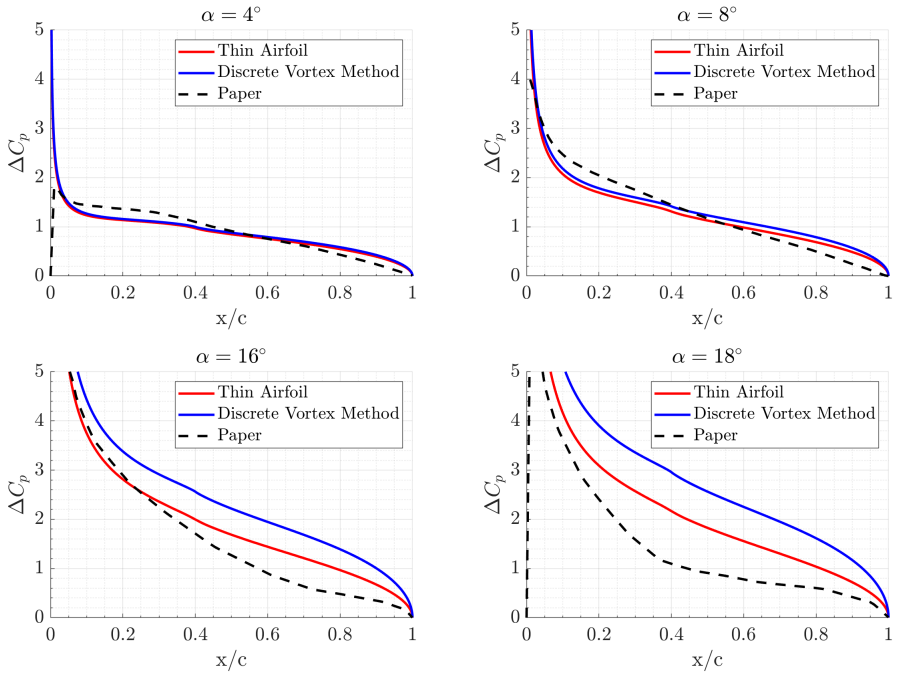

Figure 5. Comparison of the differential pressure coefficient distribution between classical thin airfoil theory, Discrete Vortex Method, and RANS simulations.

Potential Flow theory

The lift coefficient is evaluated for an angle of attack ranging from -4 to 10°. The potential flow errors compared with the numerical simulations are reported in tables 1 & 2. In general, it can be seen there is good agreement between the potential flow solutions and the reference values from the paper (Fig.6). The potential flow theory overestimates in all situations the lift produced by the airfoil The maximum absolute error is 0.149 a 10° in the case of no ground effect (Fig.6d, Table.1). The reference value of C_l is around 1.5. This corresponds to a relative error of 9.8% (Table.2).

	Absolute error for the following AoA			
Distance from the ground (h/c)	**-4°**	**0°**	**5°**	**10°**
0.4 (6a)	0.024	0.050	0.057	0.106
0.8 (6b)	0.018	0.040	0.078	0.115
1.0 (6c)	0.021	0.038	0.063	0.128
inf (6d)	0.033	0.031	0.083	0.149

Table 1. Absolute error

Distance from the ground (h/c)	Relative error for the following AoA -4°	0°	5°	10°
0.4 (6a)	0.169	0.107	0.054	0.072
0.8 (6b)	0.964	0.085	0.078	0.078
1.0 (6c)	2.584	0.080	0.062	0.088
Inf (6d)	Inf	0.064	0.081	0.098

Table 2. Relative error

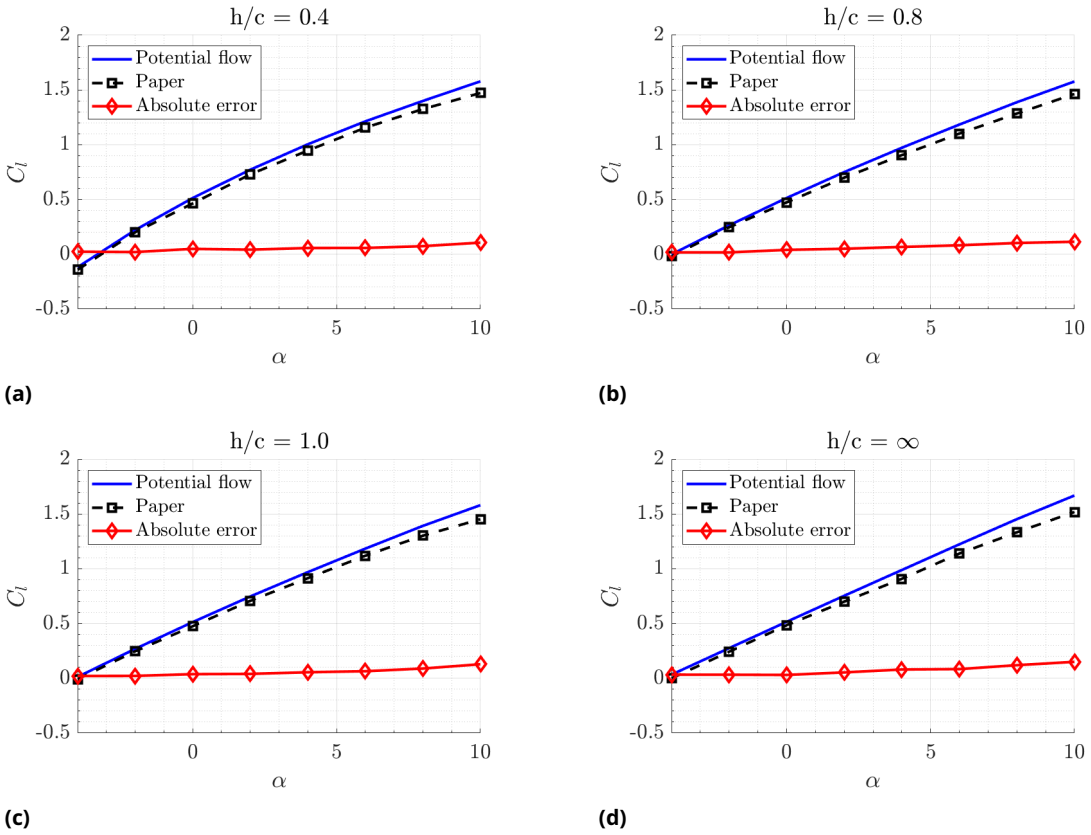

Figure 6. Comparison between lift coefficient curves between potential flow results and numerical simulations.

The absolute error for the unbounded flow solution is always greater than for finite ride heights. A similar trend is also present for the relative errors, with the only exception being $\alpha = 0°$. Therefore, the method of images can be considered sufficiently accurate in representing the effect of the ground. The error introduced by the inviscid approximation dominates over other sources of error due to the ground in the determination of the lift coefficient. As the angle of attack increases, the discrepancy between the reconstructed and reference curves grows for all ride heights. At relatively large angles of attacks viscous effects become more relevant and may not be completely neglected in the determination of pressure-based forces.

As can be seen from both the viscous simulations and the potential flow, the main effect of the ground on the lift coefficient curves is a gradual loss in linearity (Fig.7). The lift

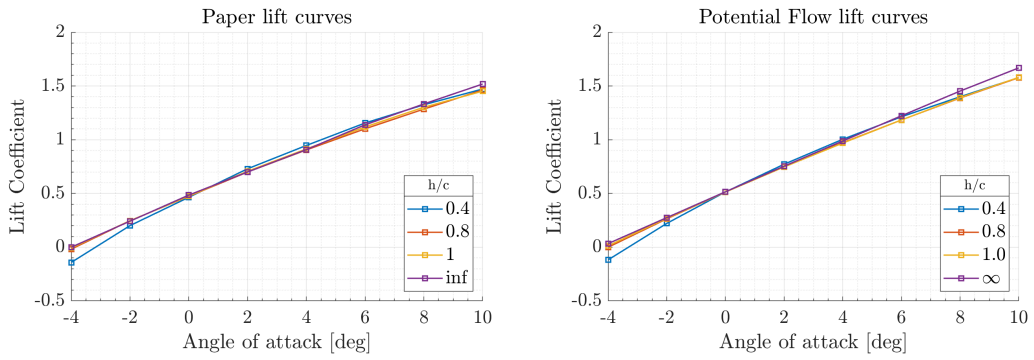

(a) **(b)**

Figure 7. Comparison of C_l-α curve (paper and potential) for different ride heights.

coefficient curves tend to become more concave the closer the airfoil is to the ground. A fixed point is present at null angles of attack. At negative angles of attack, the flow is strongly constrained between the ground and the airfoil leading edge. The flow streamlines are forced to curve more aggressively on the lower surface the closer the airfoil to the ground, thus resulting in a lower lift coefficient. For high angles of attack, the unbounded flow solution presents a higher lift than those corresponding to finite ride heights. At high angles of attacks, however, the error introduced by neglecting viscosity is larger than the variance among the lift coefficient curves. In the middle range of angles of attack ($\alpha = 0° - 5°$), potential flow captures well the slight increase in lift for small ride heights compared to the unbounded flow solution.

Conclusion

The presented inviscid theories can provide an approximation for the flow over the airfoil with or without the presence of the ground. The accuracy of these theories, when compared with RANS CFD results, is primarily influenced by the angle of attack.

The two implementations of the thin airfoil theory describe reasonably well the pressure distribution for angles of attack up to $8°$. The effect of the airfoil thickness is not negligible for a NACA4412 airfoil ($t_{max} = 0.12$) and significant deviations are present near the leading edge. Placing the vortex distribution exactly onto the camberline increases the expected lift of the airfoil. For small angles of attack, the error between the trigonometric approach and the Discrete Vortex Method is less significant than neglecting the airfoil thickness and viscous effects.

The effects of the ground on the coefficient of lift can be explained reasonably well by a potential flow theory. Deviations from the CFDs grow as the angle of attack is increased up to $10°$. In particular, the potential flow theory tends to overestimate the airfoil performance. The trend of the lift coefficient curves losing linearity and becoming more concave as the ride height diminishes is well-captured by the potential flow theory.

Work breakdown

This project is the result of a continuous shared team effort by all members. We first spent a few weeks refreshing the course material and brainstorming ideas based on the literature on the ground effect and variations of the standard thin airfoil theory.
Successively we split the work into two areas. Marion and Simon focused on implementing the MATLAB routines regarding the thin airfoil theory and Paolo on the potential flow. Even though we worked in parallel, we had continuous weekly or biweekly meetings to share our progress, resolve eventual challenges together, and provide meaningful insights and feedback.
Finally, the report has been written together on a shared Overleaf file, and the codes have been integrated into one well-structured project.

References

Abbott, Ira H and Albert E Von Doenhoff (2012). *Theory of wing sections: including a summary of airfoil data*. Courier Corporation.

DeLillo, Thomas K, Mark A Horn, and John A Pfaltzgraff (1999). "Numerical conformal mapping of multiply connected regions by Fornberg-like methods". In: *Numerische Mathematik* 83, pp. 205–230.

DeLillo, Thomas K and John A Pfaltzgraff (1998). "Numerical conformal mapping methods for simply and doubly connected regions". In: *SIAM Journal on Scientific Computing* 19.1, pp. 155–171.

DeLillo, Thomas K and Saman Sahraei (2019). "Computation of plane potential flow past multi-element airfoils using conformal mapping, revisited". In: *Journal of Computational and Applied Mathematics* 362, pp. 246–261.

Mondal, Partha and N Balakrishnan (2014). "Discrete vortex method-based model for ground-effect studies". In: *AIAA journal* 52.12, pp. 2817–2828.

Qiulin Qu, Wei Wang, Peiqing Liu, and Ramesh K. Agarwa (April 2015). "Airfoil Aerodynamics in Ground Effect for Wide Range of Angles of Attack". In: *AIAA journal* 53.4.

Sahraei, Saman (2018). "Computation of plane potential flow past multi-element airfoils using conformal mapping, revisited". PhD thesis. Wichita State University.